BRITTLE FRACTURE PREDICTION WITH THE WEIBULL STRESS APPROACH FOR NOTCHED SPECIMENS UNDER CYCLIC LOADING

TSUTOMU IWASHITA[1] and KOJI AZUMA[2]

[1] *Architecture Course, National Institute of Technology, Ariake College, 150 HigashiHagio, Omuta, Fukuoka 836-8585, Japan.*
E-mail: iwashita@ariake-nct.ac.jp
[2] *Department of Architecture, Sojo University, 4-22-1 Ikeda, Nishi-ku, Kumamoto 861-8002, Japan.*
E-mail: azuma@arch.sojo-u.ac.jp

Brittle fracture prediction is the key for prevention of occurrence of brittle fracture from weld defects and notches in steel structures. This paper describes the effects of cyclic loading on the occurrence of brittle fracture and brittle fracture prediction. Notched steel specimens were tested under monotonic loading and other five types of cyclic loadings. Two types of materials (low and high fracture toughnesses) were prepared for the specimens and all of the specimens exhibited brittle fracture. The proposed estimation methodology of cumulative ductility for predicting occurrence of brittle fracture uses the Coffin-Manson law and Miner's rule, and is based on empirical relationships between ductility amplitude and number of cycles at brittle fracture or the Weibull stress and number of cycles at brittle fracture. The proposed approach can be acceptable in predicting cumulative ductility at brittle fracture in consideration of material scatter of brittle fracture.

Keywords: Brittle fracture, cyclic loading, cumulative ductility, cumulative damage, Weibull stress.

1 Introduction

For structural engineers, a notable feature of the Kobe Earthquake was the occurrence of brittle fractures in welded joints of beam-to-RHS column connections within multi-story moment-resisting frames. A post-earthquake investigation based on a number of experiments for beam-to-RHS column connections demonstrated that cracking can be retarded by improving beam cope profiles, although the ends of complete joint penetration groove welds are particularly susceptible to weld defects (AIJ Kinki 1997). The weld defects can lead to brittle fracture because, in effect, they act as sharp-notch discontinuities and some defects induce high plastic constraint. In the research on predicting a series of brittle fracture, some specimens with a defect at the weld end showed premature brittle fracture under cyclic loading while some other specimens showed large deformation capacity although the specimens had a defect and were subjected to cyclic loading. These were related to the influence of interaction between plastic constraint and cyclic loading, which affected the occurrence of brittle fracture. We have worked on methods for predicting crack-induced brittle fracture and found that the Weibull stress approach enable us to predict the occurrence of brittle fracture more accurately (Iwashita and

Proceedings of the 17th International Symposium on Tubular Structures.
Editors: X.D. Qian and Y.S. Choo

Published by Research Publishing, Singapore.
ISBN: 978-981-11-0745-0; doi:10.3850/978-981-11-0745-0_077-cd

Azuma 2016). However, we confirmed the effectiveness of the approach under only monotonic loading.

This paper focuses on the effects of cyclic loading on plastic deformation capacity until brittle fracture with the Weibull stress approach. Notched specimens for two types of materials (low and high fracture toughnesses) were tested under monotonic loading and other five types of cyclic loading (1. constant amplitude loading, 2. monotonic loading after constant amplitude loading, 3. two-constant-amplitude cyclic loading, 4. incremental amplitude cyclic loading, 5. decremental amplitude cyclic loading). Tested under each loading were three or five specimens. All specimens led to brittle fracture. It was found that as deflection amplitude increases, cumulative plastic deformation and number of cycles at brittle fracture decreases in approximately inverse proportion although cumulative plastic deformation values show wide scatter. The Weibull stress was also used to study the effects of cyclic loading instead of deflection amplitude. Fitted curves of the relationship between the Weibull stress and the number of cycles at brittle fracture have good correlations with the experimental results for the both materials based on the Coffin-Manson law (Coffin 1954, Manson 1954).

A challenge of this research is application of cumulative damage by Miner's Rule (Miner 1945) to the specimens in this research because the Miner's Rule is basically applied for fatigue life estimation, not for brittle fracture prediction. Number of cycles at fracture was used to calculate the cumulative damage of specimens with cyclic loadings. Based on the cumulative damage, we also proposed an estimation method of plastic deformation capacity until brittle fracture, and the estimated plastic deformation capacity predicted measured plastic deformation capacity. This approach could be applied for prediction of brittle fracture from defects not only at beam-to-RHS column welded connections but also at other welded connections in tubular structures.

2 Specimens and testing procedures

2.1 *Specimens*

Figure 1 shows the specimen geometry and loading position. All test specimens are of the same geometry as shown in Figure 1. This type of the geometry is used to investigate fracture behavior, especially for brittle fracture with cyclic loading (e.g. Kuwamura and Takagi 2004). Since brittle fracture usually occurs with wide scatter, many specimens for testing are required to consider scatter. To reduce the number of the specimens, four notches are installed in each specimen. Notch root radius, ρ, is 0.15 mm in the research and the notches are symmetrically located around a loading pinhole at its centre. All are 23.0 mm thick.

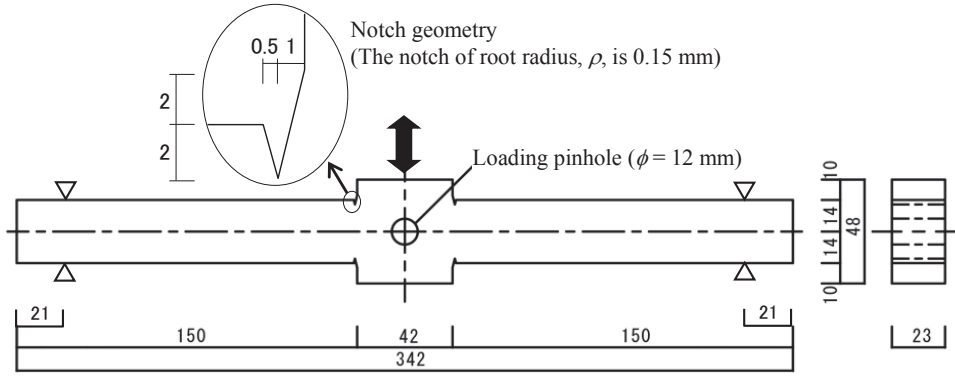

Figure 1. Specimen geometry and loading position.

2.2 *Material properties*

The samples were machined from material H (SN490B: building structural steel plate) and material L (SM490A: welding structural steel plate). Tensile and Charpy impact test results for both materials are compiled in Table 1, where $_{V}E_{-20}$ indicates absorbed energy at -20 °C, which is the test temperature in this study for both materials. As apparent in the table, material H had a high fracture toughness and material L had a lower fracture toughness.

Table 1. Material properties.

Material	Yield strength (MPa)	Ultimate strength (MPa)	uniform elongation (%)	$_{V}E_{-20}$ (J)
H	383	554	17.7	64.2
L	344	596	11.9	11.1

2.3 *Test setup and loading sequences*

Specimens were tested under monotonic loading (M) and five types of loading: constant amplitude cyclic loading (C), monotonic loading after constant amplitude cyclic loading (CM), two constant amplitude cyclic loadings (Cc), incremental amplitude cyclic loading (Ci) and decreasing amplitude cyclic loading (Cr). Loading patterns are conceptually illustrated in Figure 2 and Table 2 shows a summary of specimens and loading types. Loading was applied to the pinhole at centre of the specimens by hydraulic ram, with its head moving at a constant displacement rate until failure. M and C are basic loading procedures.

Table 2. Summary of specimens.

Specimen (Material H)	Amplitude, +/-$\Delta\delta$ (mm)	Number of specimens
M	-	3
C6.4	6.4	4
C9.6	9.6	3
C12.8	12.8	3
C20.8	20.8	3
CM6.4n4	6.4	3
CM6.4n2	6.4	3
CM8.0n2	8.0	3
CM9.6n2	9.6	2
Cc6.4n2-9.6	6.4→9.6	3
Cc6.4n4-9.6	6.4→9.6	3
Cc6.4n2-11.2	6.4→11.2	3
Cc9.6n1-6.4	9.6→6.4	3
Cc11.2n1-6.4	11.2→6.4	5
Ci	3.2→4.8→6.4 →8.0→ …	3
Cr	11.2→9.6→8.0 →6.4→ …	3

Specimen (Material L)	Amplitude, +/-$\Delta\delta$ (mm)	Number of specimens
M	-	3
C3.0	3.0	3
C3.7	3.7	5
C.4.8	4.8	3
C7.0	7.0	3
CM3.0n2	3.0	5
CM3.0n1	3.0	4
CM3.7n1	3.7	5
Ci	3.2→4.8→6.4 →8.0→ …	3

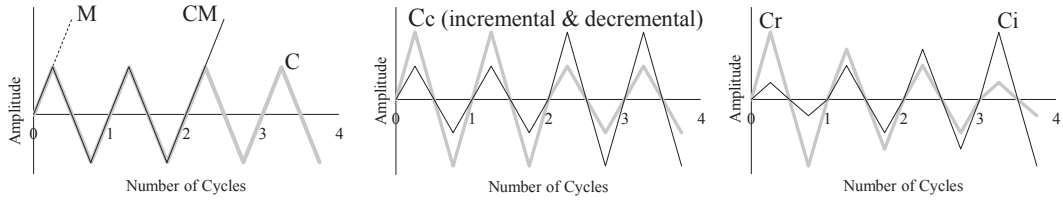

Figure 2. Loading patterns.

3 Methodology

Test results are interpreted in terms of ductility amplitude μ_p and cumulative ductility η_p. Test data are arranged in the manner of Kuwamura and Takagi (2004). For cyclic loading, average ductility amplitude μ_p is defined as

$$\mu_p = \frac{\Delta\delta_p}{\delta_p} \tag{1}$$

Here, $\Delta\delta_p$ is the average displacement amplitude (half-amplitude) and δ_p is the elastic displacement at the full plastic load, Q_p, which is obtained by the general yield point method. A definition of symbols is shown in Figure 3 (a). Because of a slight difference in $\Delta\delta_p$ by cycle during cyclic loading, $\Delta\delta_p$ was calculated as average displacement amplitude as follows:

$$\Delta\delta_p = \frac{\Delta\delta_{p1} + \Delta\delta_{p2} + \cdots + \Delta\delta_{pN}}{N} \tag{2}$$

Here, the number of cycles is different from its general definition. In this case, N is defined as the modified number of cycles and the cumulative number added one by one with an experience of the plastic deformation as shown in Figure 3 (a). N_f is the modified number of cycles at brittle fracture, and can be calculated as follows:

$$N_f = \frac{\eta_p}{\mu_p} \tag{3}$$

Thus, N_f is not necessarily an integer. η_p is cumulative ductility until fracture and is defined as follows:

$$\eta_p = \frac{\Delta\delta_{p1} + \Delta\delta_{p2} + \cdots + \Delta\delta_{p,N+1}}{\delta_p} \tag{4}$$

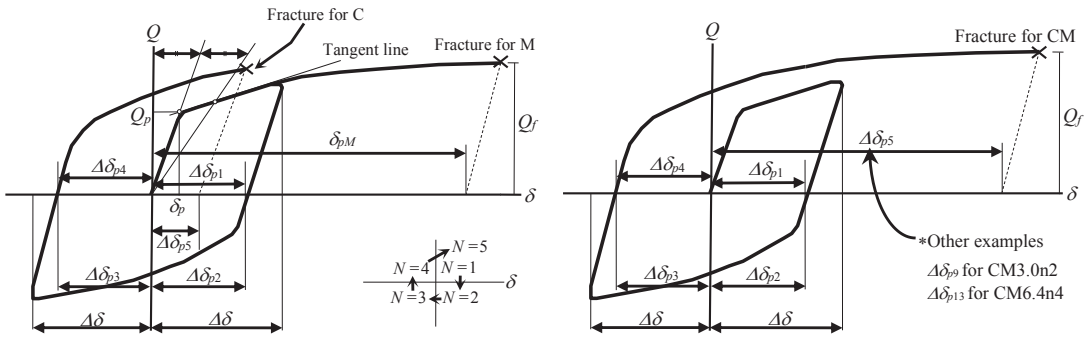

(a) Monotonic and constant amplitude cyclic loading (b) Monotonic after constant amplitude cyclic loading

Figure 3. Definition of symbols.

where $N + 1 = 5$ in the case of Figure 3 (a). η_p for the Cm loading pattern (Figure 3 (b)) is also calculated in the same way. η for monotonic loading is defined as η_{pM}:

$$\eta_{pM} = \frac{\delta_{pM}}{\delta_p} \tag{5}$$

where δ_{pM} as shown in Figure 3 (a).

We cannot directly compare cumulative ductility η_p under cyclic loading and under monotonic loading. This said, we will attempt a comparison by assuming that monotonic loading is a subcategory of cyclic loading; that is, we assume that monotonic loading is cyclic loading under which the specimen fractures during its first cycle because of a large displacement amplitude. This allows us to use η_{pM} as a measure of both ductility amplitude and cumulative ductility for the purposes of this paper.

4 Test Results

Figure 4 shows the ductility amplitude, μ_p, versus modified number of cycles at brittle fracture, N_f, of cyclic loading results (including monotonic loading results) for both materials. The figure also shows approximate equations based on the Coffin-Manson law. As μ_p decreases, N_f decreases for both materials. Also, fitted curves have good correlations with the experimental results for both materials and the values of the correlation coefficient, R, are significantly high for both materials: 0.995 for material H and 0.976 for material L, respectively. This means that the relationship between μ_p and N_f follows the Coffin-Manson law although the failure mode of all the specimens is brittle fracture.

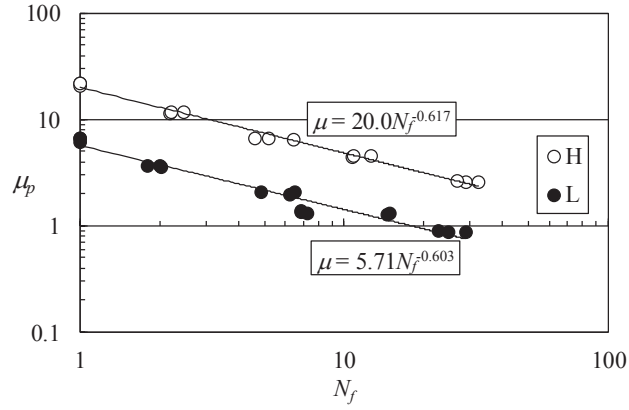

Figure 4. Ductility amplitude, μ_p, versus modified number of cycles at brittle fracture, N_f.

5 Applicability of Weibull Stress

5.1 *Weibull stress*

Measurements of fracture toughness for cleavage fractures tend to show large scatter, especially in the ductile-to-brittle transition region. This scatter is caused by a large variability in the size and extent of weak spots from one specimen to another. Here, a local approach was proposed by Beremin (1983) for statistically evaluating the behaviour of fracture toughness. This approach introduces a stress parameter σ_W, termed the Weibull stress, to represent fracture resistance in place of such conventional fracture toughness parameters as K_c, J_c, and δ_c. The Weibull stress is defined as

$$\sigma_W{}^m = \frac{1}{V_0}\int_{V_p} \sigma_1^m dV \tag{6}$$

Here, σ_1 = maximum principal stress, m = Weibull slope, and V_p = fracture process zone. The quantity V_0 is a unit volume and is usually set to 1 mm^3, and authors followed it. The Weibull slope, m, which is a shape parameter, characterizes the scatter of the Weibull stress and varies between 10 and 50 for structural steel. Typically, m has a low value in the case of low-level, broadly distributed fracture toughness. The m value is defined as 20 in this paper according to other research (e.g., Beremin 1983). Weibull stress was found to not vary for maximum principal stresses ranging from 2 σ_y and 3 σ_y; the fracture process zone, V_p, is taken to be the region in which the maximum principal stress at the crack tip is 3 σ_y or greater, because lower stresses do not contribute to the development of the Weibull stress. The fracture process zone covers the actual fracture points in the tests. The critical Weibull stress, σ_{WC}, is determined as the average value of the Weibull stress at brittle fracture of M specimens for each material: σ_{WC} = 1581 N/mm^2 for material H and σ_{WC} = 1380 N/mm^2 for material L.

5.2 *Relationship between σ_W and N_f*

Figure 5 shows plots of σ_W versus N_f. σ_W takes the value at the deflection amplitude of each specimen and this means that μ_p in Figure 4 has been replaced to σ_W in Figure 5. The figure shows that as N_f increases, σ_W decreases in approximately inverse proportion although the plots are a little scattered as compared with the results as shown in Figure 4. The fitted curves have good correlations with the experimental results for both materials and the values of the correlation coefficient, R, are significantly high for both materials: 0.994 for material H and 0.946 for material L, respectively. The results show the same tendency of Figure 4.

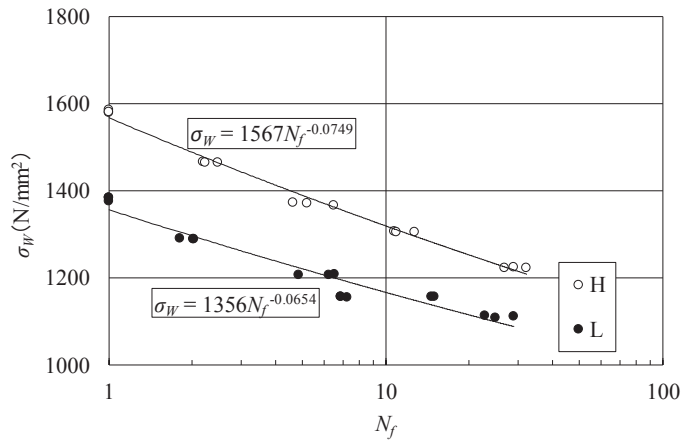

Figure 5. Weibull stress, σ_W, versus modified number of cycles at brittle fracture, N_f.

5.3 *Cumulative damage of specimens under multiple cyclic loadings*

The cumulative damage, D, based on Miner's rule is used to consider the effects of multiple cyclic loadings such as CM, Cc, Ci and Cr in the paper. Although Miner's rule is one of the most widely used cumulative damage models for failures caused by fatigue, we apply Miner's rule for estimation of occurrence of brittle fracture in low-cyclic loadings. This is also a challenging part in the study. The cumulative damage is expressed as follows:

$$D = \sum_{i=1}^{k} \frac{N_i}{N_{fi}} = \frac{N_1}{N_{f1}} + \frac{N_2}{N_{f2}} + \cdots + \frac{N_k}{N_{fk}} \tag{7}$$

Where D is the damage index, N_i and N_{fi} are the modified number of cycles and fatigue life (modified number of cycles at brittle fracture in this paper) under the i th amplitude loading, respectively. N_{fi} at σ_{Wi} (i th Weibull stress) is defined from the approximate equations in Figures 5. Values of D greater than or equal to 1.0 indicate a fracture of the specimen. As shown in Eq. (6), the equation is divided into some parts. In the case of CM specimens, N_1 is the cyclic loading part and N_2 is the monotonic loading part, for example.

Figure 6 shows the cumulative damage of the specimens under multiple cyclic loadings for both materials. Plots indicate values at brittle fracture. The average value of cumulative damages for material H is 0.960 although the all values show a little scatter. The standard deviation of cumulative damages is 0.153. Also, the average value of cumulative damages for material L is 0.945 with larger scatter and the standard deviation of cumulative damages is 0.252. The average values for the both materials are relatively close to 1.0. This means that the approach with σ_W-N_f relations and Miner's rule could be effective at evaluating occurrence of brittle fracture under cyclic loading including multiple amplitude cyclic loading. Although the values show scatter, most of the specimens with smaller D value results (D < 1.0) were subjected to larger amplitudes. For example, the CM specimens were subjected to monotonic loading after the constant amplitude loading, and amplitude of the monotonic loading part was relatively large. This should be a further research for more accurate evaluation.

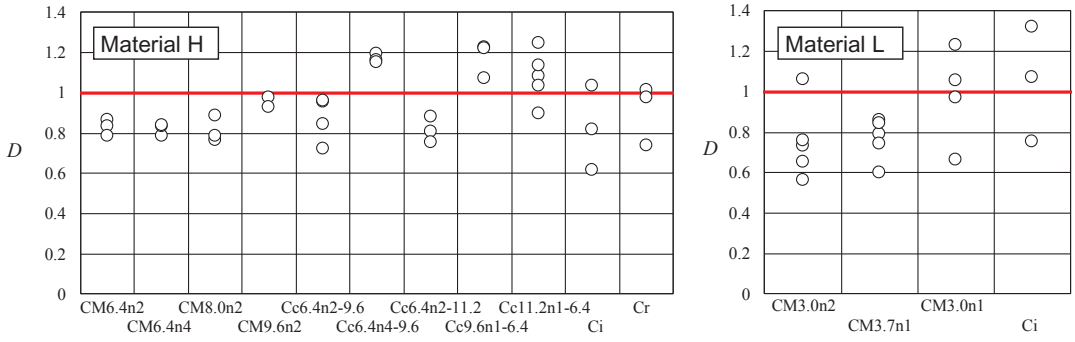

Figure 6. Cumulative damage based on σ_W -N_f relations.

5.3 *Brittle fracture prediction based on σ_W and N_f relations*

The cumulative ductility at brittle fracture were estimated for all specimens under monotonic and cyclic loading for brittle fracture prediction. To estimate the cumulative ductility at brittle fracture, the Coffin–Manson law (the σ_W-N_f relations: approximate equations in Figure 5) and Miner's rule were used in this research. We defines brittle fracture occurs when D value reaches 1.0. Figure 7 shows the relationship between tested cumulative ductility, η_{exp}, and calculated cumulative ductility, η_{cal}, for all the specimens. Although there is a scatter in material L, especially for some C specimens, the figures show a good prediction for cumulative ductility at brittle fracture. Most of the test results correspond to the calculated results and R of tested and calculated results is 0.897 for material H and 0.819 for material L. The average values of η_{exp} / η_{cal} are 0.982 and 0.975, and the standard deviation values of η_{exp} / η_{cal} are 0.136 and 0.212, respectively.

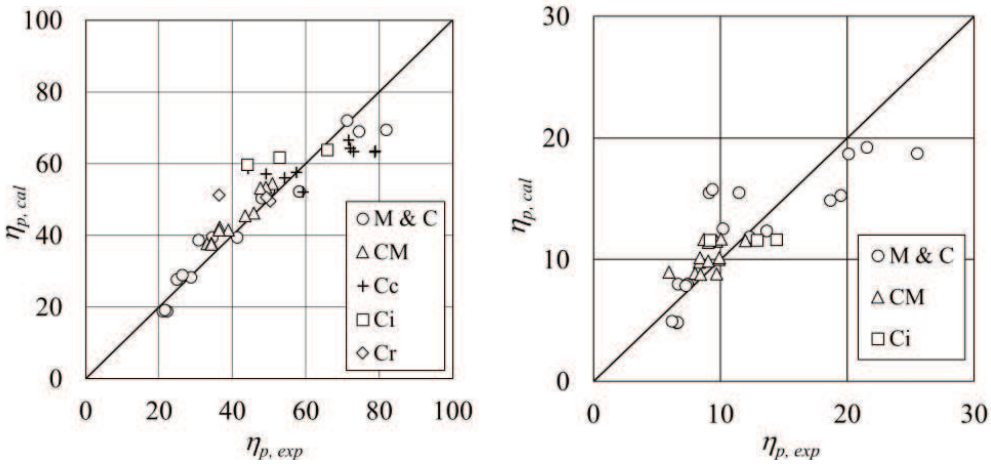

(a) Material H (b) Material L

Figure 7. Comparison of calculated and experimental cumulative ductility values.

6 Conclusions

This paper focused on the effects of cyclic loading on the occurrence of brittle fracture and described brittle fracture prediction. Notched steel specimens with low and high fracture toughness materials, were tested under monotonic loading and other five types of cyclic loading. We found that test results followed the μ_p-N_f relations and σ_W-N_f relations based on the Coffin–Manson law. According to the σ_W-N_f relations and the Miner's rule, the average value of cumulative damages for the both materials were relatively close to 1.0. Finally, the cumulative plastic deformation capacity was estimated based on the Coffin–Manson law and Miner's rule and the results showed that the calculated cumulative ductility could predict the test results.

Acknowledgments

This work was supported in part by JSPS KAKENHI Grant Numbers 16K06598, 16K06595. We would like to thank Mr. Shinji Komiya (Omuta City) for his assistance with the FEM analyses.

References

AIJ Kinki, *Full-scale test on plastic rotation capacity of steel wide-flange beams connected with square tube steel columns*, The Kinki Branch of Architectural Institute of Japan, Japan, 1997. (in Japanese)

Beremin F.M., A local criterion for cleavage fracture of a nuclear pressure vessel steel, *Metall. Trans. A*, 14(11), 2277-2287, 1983.

Coffin, L.F., A study of the effects of cyclic thermal stresses on a ductile metal, *Trans. of the ASME*, 76, 931-950, 1954.

Iwashita, T. and Azuma, K., Effects of notch sharpness and depth on brittle fractures in single-edge notched bend specimens, *Eng. Fract. Mech.*,164, 60-73, 2016.

Kuwamura, H. and Takagi, N., Similitude law of prefracture hysteresis of steel members, *J Struct. Eng.,* 130(5), 752-61, May, 2004.

Manson, S.S., Behavior of materials under conditions of thermal stresses, *NACA Technical Report 1170*, 1-34, 1954.

Miner, M.A., Cumulative Damage in Fatigue, *J. of Appl. Mech.*, 12(3), A159-A164, 1945.